Advantage of preserving bi-orientation structure of isotactic polypropylene through die drawing

Dong Lyu[a], Ying-Ying Sun[c], Yu-Qing Lai[a], Glen Thompson[d], Philip Caton-Rose[d], Phil Coates[d], Ying Lu[a*], and Yong-Feng Men[ab*]

[a] *State Key Laboratory of Polymer Physics and Chemistry, Changchun Institute of Applied Chemistry, Chinese Academy of Sciences, Renmin Street 5625, Changchun 130022, P. R. China*
[b] *University of Science and Technology of China, School of Applied Chemistry and Engineering, Hefei 230026, P. R. China*
[c] *ExxonMobil Asia Pacific Research & Development Co., Ltd., 1099 Zixing Road, Minhang District, Shanghai 200241, P. R. China*
[d] *Polymer Interdisciplinary Research Centre, University of Bradford, Bradford BD7 1DP, UK*

Abstract The isotactic polypropylene (iPP) usually showed a unique parent-daughter lamellae structure in which the parent and daughter lamellae were against each other with a near perpendicular angle (80 º or 100 º). Inducing a high fraction of oriented cross-hatched structure in iPP during processing is desirable for designing the bi-oriented iPP products. We processed a commercial iPP via tensile-stretching and die-drawing to evaluate the structural evolution of oriented parent-daughter lamellae. It turned out that the die-drawing process always had an advantage in attaining a high fraction of oriented cross-hatched structure of iPP, as compared to the free tensile stretching. Besides, the presence of α-nucleating agents affected the formation of oriented parent-daughter lamellae in the die-drawn samples whereas such influence diminished in the free stretched ones. It was found that the confined-deformation inside the die led to the well-preserved oriented cross-hatched structure in the die-drawn iPP.

Keywords Die-drawing; isotactic polypropylene; solid-state deformation; Bi-orientation; WAXD

INTRODUCTION

Isotactic polypropylene (iPP) is one of the most popular polymer materials that has been successfully commercialized due to its excellent mechanical properties and stability. [1-5] Besides the crystalline polymorphism, another feature distinguishing iPP from other polymer materials is the cross-hatched structure, which is also noted as the parent-daughter lamellae structure often found in the α form iPP. [6-10] This structure was first recognized by Khoury[6] as dendritic crystals. The dihedral angle between the parent lamellae and the affiliated daughter lamellae was suggested to be 80º[6] which was very close to the accurate value of 80º40' further determined by Padden and Keith. [7] After years of debating, [6, 8, 9] the physical essence of this peculiar parent-daughter structure was ascribed to the molecular interaction originating from chain stems chirality. [9] Lotz and Wittmann proposed that each molecular chain in the crystalline layer of α form iPP should be encircled by chain stems with different chirality. The subsequent molecular chain with the same chirality as the precursor chain in the crystallites would be pushed away, resulting in an unparallel chain arrangement in the affiliated daughter lamellae.

Attempts for inducing the oriented parent-daughter lamellae have been continually made because such structure is related to the product performance, in aspects of warpage tendency, [8] thermodynamic properties, [11] stability under shear, [12] elasticity, [13] etc. A theoretical facile method to obtain biaxially oriented polypropylene (BOPP) could be proposed based on the cross-hatched structure of iPP, [14, 15] since the angle between parent and daughter lamellae was not much different from 90º. The introduction of α-nucleating agents into iPP was an efficient approach to produce the oriented parent-daughter lamellae structure under certain conditions. [16, 17] For example, the α-nucleating agents of dibenzylidene sorbitol (DBS) family as fibril structure could first align along the force direction when shearing the compounded iPP/DBS melts, and subsequently served as oriented nuclei for inducing the growth of oriented parent-daughter lamellae by consuming the iPP melt. [18, 19] However, comparing to massive investigations on the adjustment of the daughter lamellae through modifying the polymer melt, [14, 20-22] only a few researches have been dedicated to the evolution mechanism or regulation of parent-daughter lamellae structure during solid-state deformation. [23, 24]

Nozue *et al.*[23] investigated the early deformation stage inside the spherulites and described the evolution of long periods for both parent and daughter lamellae during tensile stretching until slippage fragmentation. Li *et al.*[24]

investigated the fragmentation sequence of parent and daughter lamellae during deformation by stretching pre-oriented films at room temperature. It turned out that parent lamellae would always be destroyed first and were transformed into mesophase. In both cases, no desirable bi-oriented structure was preserved, due to the rearrangement of lamellae orientation after fragmentation. [23, 24] That means it was difficult to achieve the bi-oriented structure during solid-state uniaxial deformation even though the initial iPP samples were with a well-established oriented cross-hatched structure.

Die-drawing is one of the most ideal solid-state polymer processing techniques. [5, 25-27] Simultaneously with the elongation, the material was shaped by a specially-designed die which enabled the materials to go through a moderate strain-stress field. [25, 26] The material was also processed by the force perpendicular to the elongation induced by the die wall rather than only the drawing force. [27] Obviously, there were two forces along different directions controlling the die-drawing process. Such situation seemed to be similar to the one presented in the two-step stretching process for inducing BOPP. The difference was that the two forces belonged to the compression force and the pulling force in the former one while both of them were the tensile force in the latter case. Since the daughter lamellae were almost perpendicular to the corresponding parent lamellae, it was rational to expect different bi-oriented lamellae evolutions in samples processed by die-drawing.

In this work, we investigated the deformation of both neat and α-nucleated samples via die-drawing and tensile-stretching at different temperatures. The as-deformed samples were investigated by wide-angle X-ray diffraction (WAXD) technique to elucidate the different evolutions of oriented parent-daughter lamellar structures induced by the two distinct deformation processes. The physics behind the difference between samples deformed via different processes was deduced and the deformation scheme was illustrated.

EXPERIMENTAL

Material information and sample preparation

A commercial homo isotactic polypropylene was employed as a base material. The molecular weight (M_w) is 158,900 g/mol and the polydipersity (M_w/M_n) is 3.8. One α-nucleating agents Millad 3988i (>96% 1,3:2,4-Bis(3,4-Dimethylbenzylidene) Sorbitol (DMDBS, Milliken Inc.) and <4% Confidential Silica compound, per MSDS, version 1.3) was mixed into polymer melt along with two antioxidants, Tris(2,3-diitertibutylphenyl) phosphite and Pentaerythtieol tetrakis(3,5-di-tert-butyl-4-hydroxyhydrocinnamate). The weight ratio of the additives between the polymer melt (α-nucleating agents/two antioxidants/iPP) was 5/2/1000. Both the neat material and the α-nucleated polymer melt were further manufactured into standard injection molding bars with a length of 170 mm, a width of 10 mm, and a thickness of 4 mm. The melt temperature and mold temperature for injection molding were 200 ºC and 80 ºC, respectively. The purchase of α-nucleating agents and antioxidants, the compounding of iPP with α-nucleating agents, and the producing of injection molding bars were all carried out at ExxonMobil. All the injection molding bars were further cut into sample bars with a width of 5.5 (±0.3) mm to fit in the mini die-drawing setup.

Differential scanning calorimeter (DSC)

The crystallization temperature, melting points, and crystallinities of the iPP samples were measured by using DSC (DSC1 Star^e System, Mettler Toledo, Swiss) technique at a cooling or heating rate of 10 K min^{-1}. For the compounded sample of iPP/α-nucleating agents, it showed a crystallization temperature of 131.5 ºC which was much higher than the one of 112.4 ºC observed in the neat iPP during cooling down from the molten state. For the injection-molded iPP samples, a larger crystallinity of 51% and a higher melting temperature of 167.1 ºC could be found in the α-nucleated iPP than that of 44% and 166.5 ºC in the neat iPP. The crystallinities were determined by dividing integral area of endothermic peak by the theoretical heat fusion value of perfectly crystallized iPP. [28] It confirmed that the low content of α-nucleating agents of DMDBS was efficient in promoting the crystallization of iPP. [29]

Polarized optical micrograph (POM)

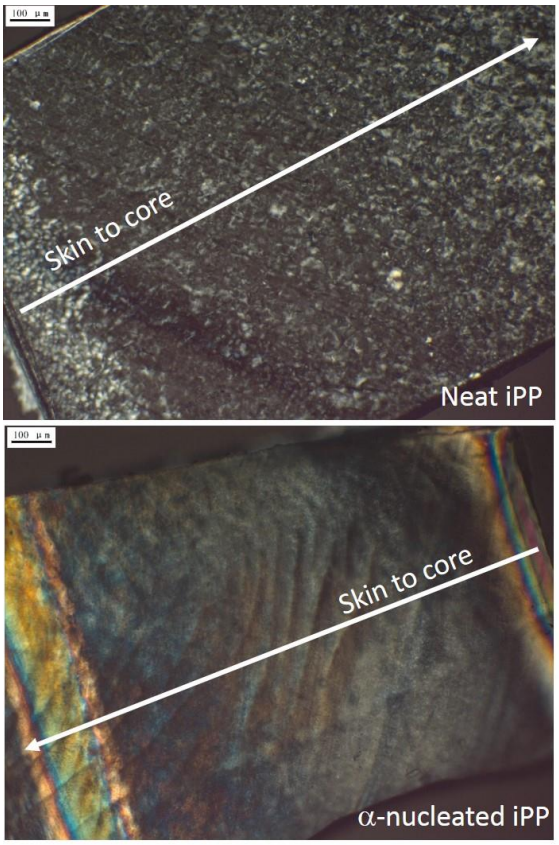

Fig. 1 POM images of the injection-molded neat iPP (top) and α-nucleated iPP (bottom). The arrows on the plot represent the direction perpendicular to the flow direction during injection. (Scale bar: 100 μm)

The optical micrographs were captured through Axio Imager A2m (Carl Zeiss, Germany) under the cross-polarized light, the morphologies of injection-molded iPP samples from the

skin area to the core region are revealed in Fig. 1. The neat iPP formed the spherulitic structure, while the α-nucleated one presented the oriented structure at the skin and core regions as evidenced by the color stripes. In general, the core layer of injection-molded iPP normally showed the spherulitic structure due to the poor orientation of molecular chains. [30] The well-developed oriented lamellae, however, had been observed in the core region of injection-molded iPP compounded with DMDBS in our case. It was clear that the DMDBS could encourage the growth of oriented lamellae, which was in line with the findings figured out by Lipp *et al.* [19]

Deformation tests

All the samples were deformed beyond necking with a drawing/stretching speed of 94 mm min^{-1} at 130, 140, and 150 °C via die-drawing and tensile-stretching processes, respectively. The die-drawing experiments were performed via a self-designed mini die-drawing setup, and the whole view of this setup could be found in our previous work. [27] As schemed in Fig. 2, the die with a heating system was designed with a tilted angle of 15° to the deformation direction which could provide the compression force (N) and the friction (f) to weaken the drawing force (F_d). In this simplified model (right of Fig. 2), the sample was controlled by both of the force parallel and the one perpendicular to the deformation direction inside the die. The major shaped area of sample during die-drawing was inside the die because the temperature out of the die was room temperature far below the deformation temperature inside the die. The pull-out region of die-drawn sample normally showed the similar macroscopic state, as highlighted by the black rectangle in the left of Fig. 2.

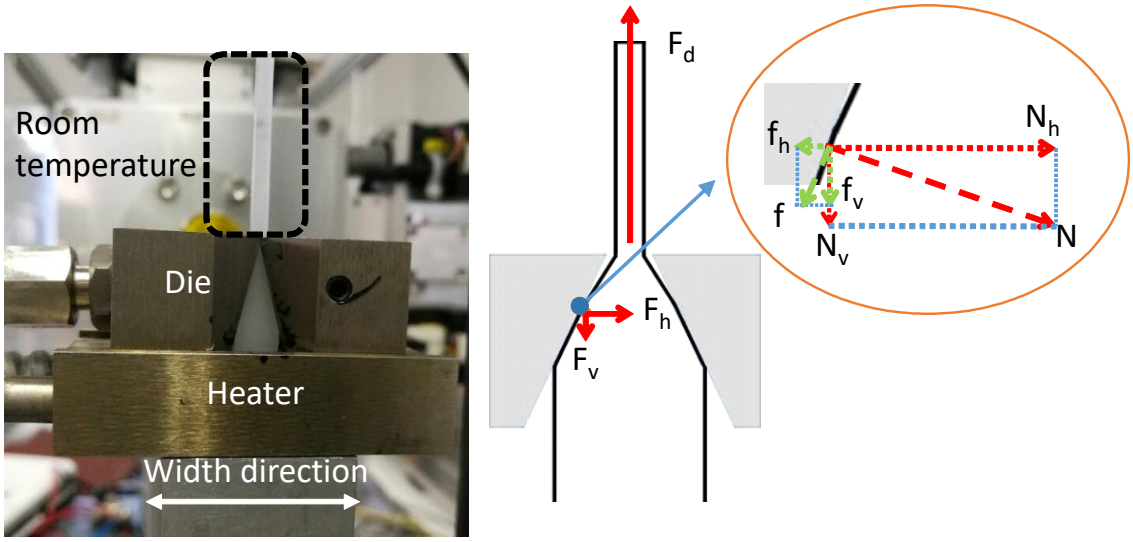

Fig. 2 The details of the die of mini die-drawing setup (left) and a schematic representation of the force distribution inside the die along the width direction (right). F_d, N, and f refer to the drawing force, the compression force from the die wall, and the friction caused by the die wall. The N and f can be orthogonally decomposed to the N_h, N_v, f_h, and f_v (right inset). These four forces are finally reconstructed to the force of F_v (parallel to the F_d) and F_h (perpendicular to the F_d) in order to simplify the force distribution inside the die.

For the free tensile stretching tests, an electronic universal testing machine (Instron 5869, Instron, USA) equipped with heating oven was employed. Prior to deformation, all the samples were kept at the deformation temperature for 20 minutes to gain a homogeneous heat distribution. The intended deformation temperatures were 130 °C, 140 °C and 150 °C, but it turned out the actual deformation temperatures were 130 °C, 140 °C and 145 °C due to the temperature deviation at high temperature. Although the initial crystallinities of neat and iPP/DMDBS samples were different, the high temperature annealing could melt the disordered crystallites and these melts would recrystallize into more perfect crystallites. Thus, we found the crystallinity difference between the neat and α-nucleated samples was approximately decreased from 7% to 3% before stretching due to the 20 minutes annealing effect. The deformation degree of the as-deformed samples was evaluated via actual deformation ratio, R_A. [25]

$$R_A = \frac{\textit{Original billet cross-sectional area}}{\textit{Final product cross-sectional area}} \qquad (1)$$

Photos were taken before and after the sample deformation along with a steel ruler to record the variation of both the width and thickness of the samples. In addition, the cross-sectional area at the die exit was 2 (width) × 5 (thickness) mm^2, so that the final R_A of die-drawn iPP samples mainly depended on the initial width since the initial thickness of sample was 4 mm.

WAXD

A customized micro-focus WAXD setup was employed to investigate the structure evolution of samples. This setup

consists of a micro-focused Cu K□ X-ray source (GeniX^{3D}, Xenocs SA, France) which was generated at 50 kV and 0.6 mA and a semiconductor detector with a resolution of 487×195 (pixel size =172 × 172 μm^2) (Pilatus100 K, DECTRIS, Swiss). The sample-to-detector distance was around 50 mm and the size of the X-ray beam at the sample position was 40 × 60 μm^2. The acquisition time for each two-dimensional (2D) WAXD pattern was 60 s. The orientation degree of polymer chains and fractions of oriented parent lamellae were further calculated based on one-dimensional integrated curves obtained from 2D WAXD patterns.

The orientation degree of polymer chains were calculated via Hermans equation: [31]

$$S_{hkl} = \frac{3<cos^2\phi_{hkl}>-1}{2} \qquad (2)$$

where ϕ_{hkl} represents the angle between the deformation direction and the normal vector of the lattice plane (*hkl)*. The orientation parameter $cos^2\phi_{hkl}$ can be achieved from azimuthal scattering intensity distribution by the following equation:

$$cos^2\phi_{hkl} = \frac{\int_0^{\pi/2} I_{hkl}(\phi)cos^2\phi sin\phi d\phi}{\int_0^{\pi/2} I_{hkl} sin\phi d\phi} \qquad (3)$$

where $I_{hkl}(\phi)$ describes the scattering intensity along the angle ϕ. And ϕ can be obtained by using Polanyi equation: [32]

$$cos\phi_{hkl} = cos\theta_{hkl} cos\psi \qquad (4)$$

where θ_{hkl} denotes the Bragg scattering angle, ψ is the azimuthal angle along the Debye circle. In this work, we chose the polymer chains in the $(040)_\alpha$-lattice plane to evaluate the orientation degree of the system, which made θ_{hkl} 8.4° according to the characteristic peak position of iPP $(040)_\alpha$ lattice. [33]

In the case of a perfect orientation of the lattice plane with its normal in the plane of equator, the order parameter *S* is equal to -0.5. For an isotropic sample, the order parameter *S* is usually 0. If the molecular chains are entirely oriented perpendicular to the polar direction, the value of *S* is close to 1. However, in this work, the orientation parameter of (*hk0*) planes can vary in the range from 0 to -0.5 since we only consider the alignment of molecular chains from its isotropic state to perfectly oriented one along the polar direction, as the normal of such planes are generally perpendicular to chain direction. The closer the value of *S* to -0.5, the higher the orientation level is achieved for the corresponding lattice plane.

As for evaluation on the fractions of parent lamellae (f_{parent}), the following equation[34] was employed after baseline subtraction:

$$f_{parent} = \frac{A_{parent}}{A_{parent}+A_{daughter}} \qquad (5)$$

A_{parent} represents the peak area of the parent lamellae diffraction peak which in this work was the peak around 90°, and $A_{daughter}$ represents the peak area of the daughter lamellae diffraction peaks around -10° and 10° azimuthally. The crystallinity, the sum of parent and daughter lamellae, at different positions was calculated based on Gaussian fitting of both the crystallographic sharp diffraction peaks and the broad peak originated from amorphous region, as introduced in our previous work. [35]

Small angle X-ray scattering (SAXS)

In order to express the long spacing d_{ac} of deformed iPP samples, the SAXS measurements were conducted with a modified Xeuss system of Xenocs, France, at a sample-to-detector distance of 1064 mm. The size of X-ray beam (Cu K_α X-ray source, λ=0.154 nm) was enlarged to 0.8 × 0.8 mm^2 during exposure. For scanning the drawn iPP samples from the undeformed area to the deformed region, the stepwise scanning with an interval of 1 mm was employed. Each 2D SAXS pattern was collected within 30 minutes using the same detector mentioned in the WAXD technique. The 1D radial scattering intensity profiles were first obtained by integrating the background corrected 2D SAXS patterns within ± 20° along the machine direction. The value of long spacing d_{ac} was then computed by using the Bragg equation based on these 1D scattering curves.

$$d_{ac} = \frac{2\pi}{q_{max}} \qquad (6)$$

RESULTS AND DISCUSSION

Orientation of molecular chains during deformation

Selected 2D WAXD patterns of samples are presented in Fig. 3 and the corresponding characteristic α crystalline diffraction rings are indicated as well. Although the β phase of iPP samples could be occasionally induced during the injection molding process, [36] no β crystalline form could be traced in the current work. The 2D WAXD patterns of all the samples started from almost isotropic rings but still accompanied by slight orientation which originated from the injection molding process. [37] The molecular chains in the iPP melt could be oriented along the flow direction during injection which would act as the nucleation sites for inducing the crystallization of oriented lamellae. Moreover, the α-nucleating agents would be also oriented along the flow direction together with the formation of oriented iPP molecular network, both of them accelerated the growth of anisotropic lamellae. With deformation ongoing, the strongly focused diffraction spots or arcs progressively appeared on each diffraction ring. Those intense diffraction spots or arcs manifested a preferential orientation of polymer chains within crystallites. Several 2D WAXD patterns of tensile-stretched samples were also born with a tilted feature (e.g., R_A= 2.08 in Fig. 3 (c)) which came from sample inclination and were corrected by positioning the maximum diffraction point of $(040)_\alpha$-lattice plane at 90° before further calculation.

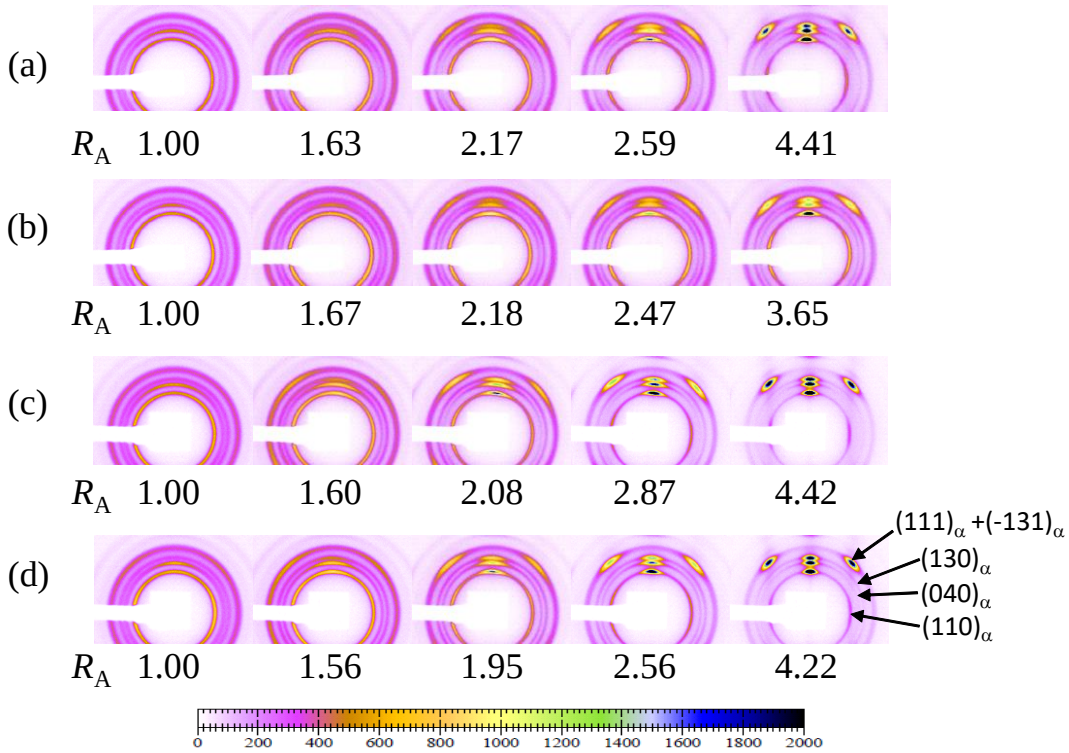

Fig. 3 Selected 2D WAXD patterns of samples deformed at 130 °C via different processes. The top two rows were the patterns of die-drawn samples and the other two were for tensile-stretched samples. (a) and (c) represented the neat samples while (b) and (d) were for α-nucleated samples. Deformation direction: horizontal.

To quantify the orientation evolution of the deformed samples, the order parameter of $(040)_\alpha$-lattice plane, $S_{(040)}$, was calculated as descripted in the experimental section and the results are presented in Fig. 4. The orientation degrees at one same R_A of stretched samples through different deformation approaches are highlighted by the arrows in the figure. Firstly, same as the results indicated by the 2D WAXD patterns, all the samples were oriented better than their original states after deformation. Secondly, tensile-stretching process could feature better orientation level than die-drawing process for all samples with or without nucleating agents. Thirdly, although the starting orientation degree was similar for the neat samples and the α-nucleated samples, the former exhibited better orientation after die-drawing process ($S_{(040)}$ = -0.30 and -0.24 at R_A of 3.8). On the other hand, the difference between the neat and the α-nucleated tensile-stretched samples was not evident ($S_{(040)}$ = -0.35 and -0.35 at R_A of 4.7). Fourthly, the free stretched iPP at a higher deformation temperature favored in obtaining a higher orientation at an earlier R_A. This behavior could be associated with the higher molecular chains mobility at a higher temperature, which strengthened the large scale of melting and recrystallization of lamellae in advance. [38] Such influence of deformation temperature on the orientation of die-drawn iPP samples was intensively reduced.

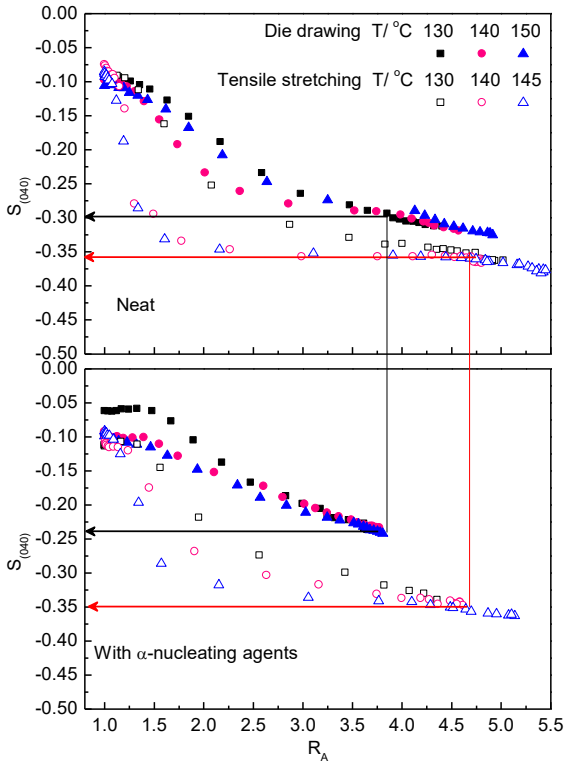

Fig. 4 The $(040)_\alpha$-order parameter of samples deformed at different temperatures via two processes. The top one represents the neat samples and the bottom one depicts the α-nucleated samples.

In a whole, the method of processing could affect the microstructure evolution of iPP during deformation and more importantly, the microstructure induced during deformation could also be influenced by the initial structure of iPP during die-drawing. One thing should be emphasized that, the α-nucleated iPP samples presented a smaller value of final R_A than the neat iPP samples, which was caused by the smaller initial width of the α-nucleated samples.

Evolution of oriented parent-daughter lamellae during deformation

To calculate the content of oriented parent lamellae of different samples, ring integral was applied on the $(110)_\alpha$ lattice plane diffraction ring and the 1D curves of neat samples are depicted in Fig. 5. The integral azimuth ranged from -50 ° to 130 ° since the diffraction signal of the parent-daughter lamellae is symmetrical. The angle between a set of parent and daughter lamellae was around either 80 ° or 100 °, bringing out different diffraction signal azimuth angles on the diffraction ring of $(110)_\alpha$ lattice plane. But at the isotropic state, the signal of parent lamellae and daughter lamellae would merge as the black curve in Fig. 5. The intensity distribution along the azimuth angle was approximately even making it impossible to distinguish the parent lamellae and daughter lamellae. Thus, we could exclude the isotropic cross-hatched structure by subtracting the baseline of these azimuthal integrated profiles in Fig. 5. The rest intensities of the subtracted profiles were predominantly devoted by the oriented lamellae and the fraction of oriented parent lamellae could be obtained through equation 5. The lamellae with normal parallel to the elongation direction were defined as parent lamellae.

Inspecting the intensity's azimuthal profiles, one finds a gradual reduction of the intensity with increasing the R_A, except for at the azimuth angles perpendicular to the stretching direction which is also the location of final parent lamellae. It should be made clear that only part of the lamellae with normal along the stretching direction belong to parent lamellae because most of the newly formed oriented lamellae due to stress induced melting and recrystallization does not show strong ability of inducing daughter lamellae. This is better seen from the data presented in azimuthal intensity distribution of $(110)_\alpha$ of the free stretched sample in the bottom chart of Fig. 5. Globally, free stretching intends to destroy all existing crystalline lamellae regardless parent or daughter ones along all directions and transforms all freed polymeric chain segments into highly oriented lamellae with normal along the stretching direction. As a result, to the extent of current deformation ratio, only a small fraction of diffraction due to daughter lamellae adhered to the parent lamellae previously already possess an orientation with the normal along stretching direction. Comparing data of die-drawn and free stretched samples presented in Fig. 5, one immediately recognizes that a larger fraction of daughter lamellae can be observed in the die-drawn sample at the same deformation. This suggests strongly that a preferential preservation of the original parent and daughter lamellae originally already possess such orientation has been realized via die drawing. In addition, the crystallinity almost stayed unchanged during all the deformation case, as included in Fig. S1 in the supporting information. Such a result could be assigned to the high deformation temperature favoring the formation of ordered crystallites, which would not decrease the crystallinity of sample initially featured with high crystallinity. The R_A was not high enough to induce the disentanglement of the oriented amorphous network which can be recognized through the large strain cavitation, [5] so the crystallinity hardly increased.

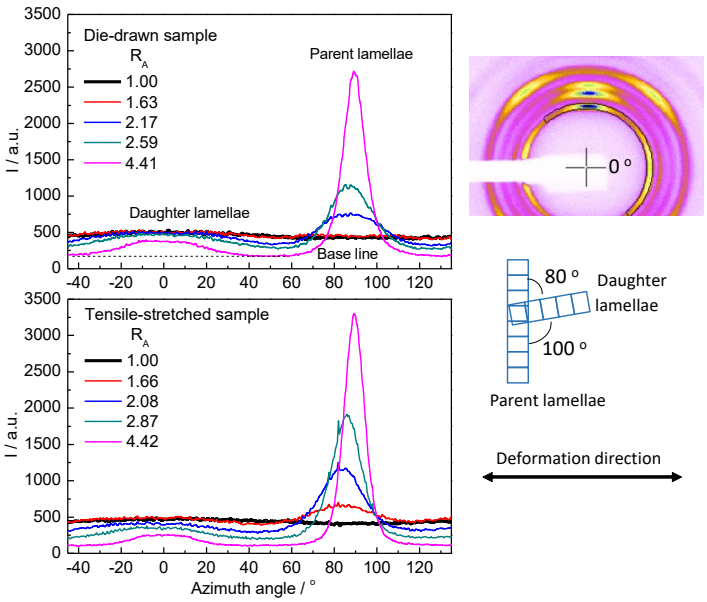

Fig. 5 Selected ring integral curves of die-drawn (top) and free stretched (bottom) samples deformed at 130 °C at different deformation stage. The 2D WAXD pattern shows the integrated azimuthal angle at the $(110)_\alpha$ lattice plane. The schematic of parent-daughter lamellae is given in the right.

Fig. 6 depicts the evolution of oriented parent lamellae fractions of samples deformed via different modes. The solid and hollow symbols represent the results of die-drawn and tensile-stretched samples, respectively. These fractions are relative values not the absolute ones in the whole system since the randomly distributed lamellae have not been considered in accounting for the meaning of the baseline subtracted in Fig 5. However, the oriented lamellae increased with consuming the isotropic lamellae as the R_A increased, it means the fractions of oriented parent lamellae given in Fig. 6 became much closer to the absolute values in the whole system at the final deformation region. At the initial deformation stage, the α-nucleated samples had an average value of 20% oriented parent lamellae which was slightly higher than the neat iPP samples with 12 %. It confirmed that the α-nucleating agents DMDBS promoted the evolution of oriented lamellae during injection. With increasing the R_A, the oriented parent lamellae of all the neat iPP samples kept increasing along with the draw ratio, indicating that the melting of original crystallites and recrystallization of new crystallites with normal parallel to the drawing direction took place. Although the fraction of oriented parent lamellae in the α-nucleated samples first gave a slight decrease at the early deformation stage, the final fraction still increased. Considering that the α-nucleated samples contained larger fraction of oriented parent lamellae after injection, these oriented lamellae could be regarded as the load-bearing subjects at the beginning of deformation. We thus observed an early decrease of the content of oriented parent lamellae in the α-nucleated samples due to the breakage of the original oriented parent lamellae. Besides, both deformation processes exhibited critical turning points which were used to reflect the rate for inducing the oriented lamellae. Before these critical points, the oriented parent lamellae were born with a fast rate. Beyond these points, the growth rate of oriented lamellae suddenly slowed down. In a detailed analysis, the difference of the oriented parent-daughter lamellae developed during different deformation processes could be summarized as follows.

(I) In terms of the results of the neat samples shown in the top of Fig. 6, the turning points for obtaining a larger amount of the oriented parent lamellae in the tensile stretched iPP and the die-drawn samples were at the R_A around 1.35 and 2.61, respectively. The R_A of 1.35 was matched with the necking position of free stretched samples and the one of 2.61 was not far away from the corresponding die exit position on the die-drawn samples. Because the melting and recrystallization was mainly activated at the position of necking, [39] the increase of the oriented parent lamellae of iPP samples became much slower at the R_A larger than 1.35 during free stretching. For the die-drawn sample, the main deformation area was inside the die. The oriented parent lamellae therefore increased slightly as the R_A larger than 2.61 where it was the region outside of the die. Furthermore, we also found that the final parent lamellae fractions of samples deformed via tensile-stretching were larger than the ones of die-drawn samples regardless of deformation temperature, indicating a less content of oriented cross-hatched structure was built in the former case.

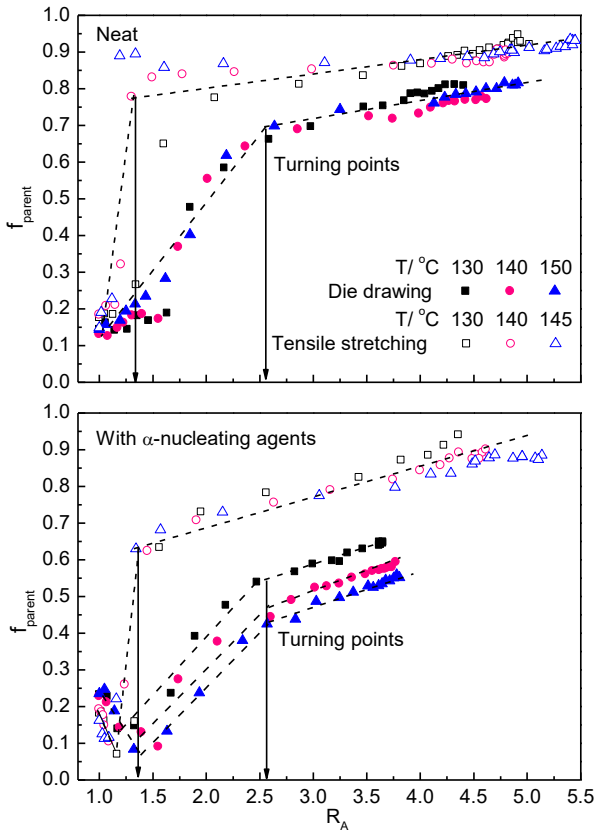

Fig. 6 The evolution of oriented parent lamellae fractions of samples deformed at different temperatures via two deformation processes. The top one was the results of neat samples and the bottom depicted the results of samples with α-nucleating agents. (Error bar: within 4 %)

(II) The performance mentioned above could also be found in the α-nucleated samples. In the case of free stretched samples, both the neat and nucleated samples showed the same turning points around the R_A of 1.35. The final fractions of oriented parent lamellae in these two samples almost reached 90 % notwithstanding the difference at the beginning. However, there were certain differences as comparing the neat and α-nucleated samples deformed through the die-drawing. It was clear that the final oriented parent lamellae fractions of the neat ones were larger than the α-nucleated ones during the whole deformation. The deformation temperature influenced the formation of the oriented parent lamellae of α-nucleated iPP as well. A higher stretching temperature preferred in forming a smaller fraction of oriented parent lamellae. In addition, the turning point at the R_A of 2.50 in the α-nucleated samples was slightly smaller than the one observed in the neat samples during die-drawing. Such result was attributed to the smaller R_A of α-nucleated iPP samples at the out gate of die.

Combined the results given in Fig. 4 and Fig. 6, it could be concluded that the die-drawing process was in favor of the preservation of oriented parent-daughter lamellae and the existence of α-nucleating agents further enlarged the content of the oriented parent-daughter lamellae of die-drawn samples. A higher deformation temperature was also beneficial for

obtaining an appropriate content of oriented cross-hatched structure in the die-drawn iPP. In contrast, the drawing temperature and the α-nucleating agents hardly affected the final fraction of oriented parent lamellae of iPP during free tensile stretching. All the iPP samples showed 90 % oriented parent lamellae at the late deformation stage. Evidently, the die-drawing process had an advantage in obtaining the oriented cross-hatched structure, especially at high deformation temperature. In other words, it could be expected to achieve bi-orientation lamellae in iPP through die-drawing.

Another thing should be emphasized, the turning points observed in Fig. 6 could also be found in Fig. 4, but the values of R_A at the turning points in Fig. 4 were beyond the necking position for the free stretched samples. For example, the turning point of orientation parameter in the 140 and 145 ºC free stretched cases was around R_A=1.7. It can be understood if we look deep into the calculation methods of the orientation parameter and the fraction of oriented parent fraction. In the case of orientation parameter (Fig. 4), it is a result of the arrangement of all molecular chains in the whole system. For the fraction of oriented parent lamellae (Fig. 6), only the oriented lamellae are considered and the fraction of randomly distributed lamellae has been excluded. Especially, the oriented lamellae only possessed a small fraction in the whole system at the early deformation stage. So we observed a later turning point in Fig. 4 since the large scale rearrangement of molecular chains in the whole system could not be finished at the necking position. For the die-drawn iPP samples, the turning points for orientation parameter in Fig. 4 were similar to these found in Fig. 6. As discussed above, the factions given in Fig. 6 could represent the absolute values in the whole system at the large R_A. It means that both the orientation parameter and the fraction of oriented parent lamellae reflected their counterpart situations in the whole system at large R_A. So the turning points for the orientation parameter and for the fraction of oriented parent lamellae in iPP during die drawing were coincided with each other.

The cause for a high fraction of bi-oriented structure in die-drawn iPP

As well-known, the plastic deformation of semi-crystalline polymers was supposed to be controlled sequentially by two dominant mechanisms, the first one defined as crystalline slippage and the successive one noted as melting-recrystallization. [40] At the early stage of deformation, i.e. around yield, the crystalline layers would slip to keep up with the macroscopic shape change. Beyond that, the melting and recrystallization of crystallites would take place. The stress imposed on the crystalline block progressively increased along with deformation and finally caused the mechanical melting. Crystalline layers or crystallites would be further degraded into smaller pieces so that molecular chains could relatively be freed and realign along the stretching direction to generate new crystallites.

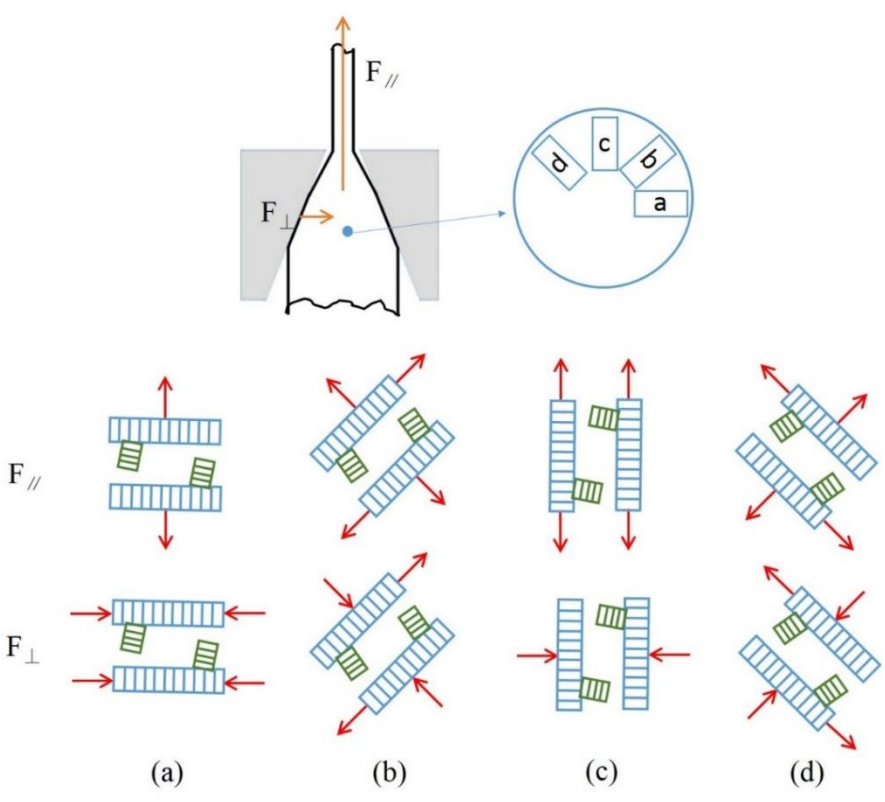

Fig. 7 The force applied on the lamellae during die-drawing process at four representative positions inside the spherulites. $F_{//}$: Force parallel to the elongation direction. $F_{\perp}$: Force perpendicular to the elongation direction. Red arrows represented the resolved effect of either $F_{//}$ or $F_{\perp}$ along and perpendicular to the normal of parent lamellae.

For understanding the difference observed in samples deformed via two deformation modes, the relative optimal deformation path induced by the die in die-drawing process was primarily considered. [26] During deformation the existence of die could contain the stress applied on the samples at a relatively low level comparing to tensile-stretching method. [26] Clearly, the stress was the intrinsic reason of the adjustment of molecular chains and crystalline destruction. In our previous work, [27] the forces applied on the samples during die-drawing process were resolved into parallel and perpendicular forces to the elongation direction, as illustrated in Fig. 2. In contrast, the stress was only applied along the machine direction during the tensile stretching process. The underlying reason that made the different results of samples prepared by these two methods should come from the different forces applied on the samples.

Inspired by the work addressed by Aboulfaraj *et al.*, [41] the force applied on the lamellae at different positions inside the spherulite were analyzed in the case of die-drawing process. To gain a clearer look, the forces parallel and perpendicular to the drawing direction were further transformed into forces parallel and perpendicular to the normal of parent crystalline layers and the details are presented in Fig. 7. $F_{//}$ and $F_{\perp}$ represent the force along the elongation direction and the one perpendicular to the drawing direction, respectively. The longer rectangles represent the original parent lamellae, while the shorter ones depict the affiliating daughter lamellae. Clearly, the forces along different directions had different effects on the lamellae at different positions ((a) equatorial region, (c) polar region, (b) and (d) diagonal region) of the spherulites.

As shown in Fig. 7, the $F_{//}$ tended to separate and subsequently destroy the adjacent parent lamellae at position (a), promoting the rearrangement of molecular chains along the deformation direction. At position (b) and (d), the effect of the force was similar, tending to slide the lamellae against each other and successively destroy the lamellae at the same time. Then, the molecular chains recrystallized into the new lamellae with normal parallel to the $F_{//}$ direction. At position (c) the force would stretch the parent lamellae along the direction perpendicular to the molecular chains which was in favor of the crystalline destruction in the following melting-recrystallization process.

$F_{\perp}$, by contrast could induce distinctive different influences on the lamellae at above-mentioned positions. Compressional force was supposed to be found in the lamellae at position (a) which could help keep the integrity of the parent lamellae. Although both $F_{//}$ and $F_{\perp}$ would lead the adjacent lamellae slide against each other at position (b) and (d), the latter one would push them together instead of separating them. Such effect would make it be harder for the adjacent parent lamellae to slip against each other and be mechanical melted, possibly leading to a bad reorientation along the force of $F_{//}$. The lamellae at position (c) would be pressed together as well due to the $F_{\perp}$. In summary, it seemed that $F_{\perp}$ could weaken the effect of $F_{//}$. As a consequence, the die-drawing process could not provide the efficient stress for melting the original lamellae and generating the new lamellae with normal along the $F_{//}$ direction.

As for the tensile-stretched samples, it was not difficult to deduce that similar but not the exactly same effect of $F_{//}$ was achieved during the tensile-stretching process. Comparing to the die-drawing process, larger stress was required during the tensile-stretching process at high strains. [25, 26] Because the stress should be strong enough, the melting of original lamellae and the recrystallization of new lamellae could be proceeded during deformation. [38] The stress applied on the lamellae of iPP during free stretching was apparently larger than the one during die-drawing in account of the absence of $F_{\perp}$. Hence, less original lamellae at any direction could be preserved and more new lamellae along the force direction were born in the iPP during free tensile test. We thus observed a higher oriented parent lamellae fraction and a better orientation of molecular chains for the free drawn iPP at the final deformation stage, as shown in Fig. 4 and Fig. 6. The different behaviors found between samples deformed via different processes were supposed to be mainly originated from the $F_{\perp}$, the force perpendicular to the elongation direction.

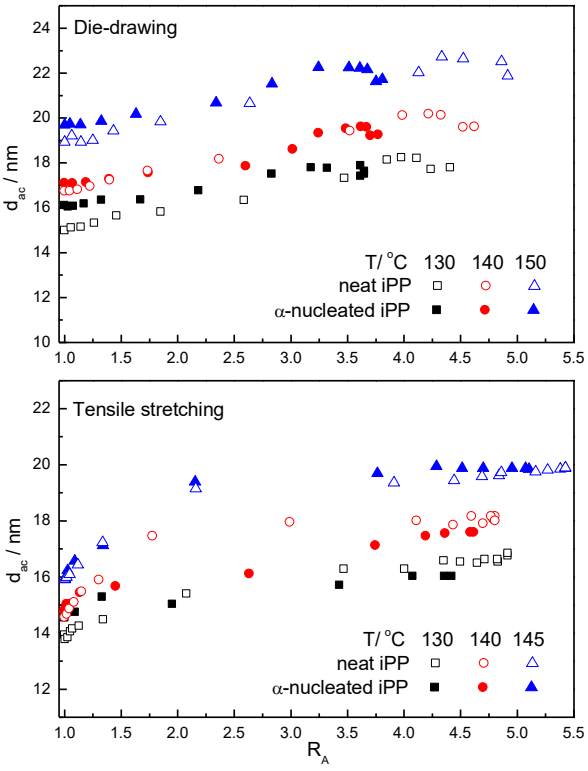

Fig. 8 The evolution of long spacing d_{ac} against the deformation ration R_A at different deformation cases. (Error bar: within 0.9 nm)

With respect to the difference between the neat and the α-nucleated samples deformed via the same process, the existence of α-nucleating agents could elevate the crystallization temperature during injection molding[33] as evidenced by the higher crystallinity and the larger long spacing displayed in Fig. 8. In the situation of free stretching,

the stress exerted upon the lamellae was high enough for inducing the melting and recrystallization of original crystallites. It could be envisaged that most of the original lamellae could be melted and recrystallize into the new ones during free stretching. The initial microstructures, such as a high crystallinity and a large value of d_{ac}, had no effects on the final content of oriented parent lamellae and the orientation of molecular chains. Accordingly, both the neat iPP and the α-nucleated iPP presented the similar fractions of oriented parent lamellae and orientation degree of molecular chains at the later deformation region.

In the case of die-drawing, the melting and recrystallization of original lamellae had already become difficult due to the less sufficient force of $F_{//}$ weakened by the one of $F_{\perp}$. The breakage and recrystallization of thicker lamellae should require a larger stress, as being confirmed in our previous work. [38] Therefore, the fragment and recrystallization of the α-nucleated iPP born with thicker lamellae was limited during die-drawing. The number of newly-created lamellae with normal parallel to the $F_{//}$ in the α-nucleated iPP became less, so that we observed a smaller fraction of oriented parent lamellae after die-drawing.

Additionally, a higher deformation temperature could also increase the initial d_{ac} of iPP due to the annealing effect, as evidenced by the results in Fig. 8. The corresponding results further influenced the fraction of oriented parent lamellae in the α-nucleated iPP during die-drawing. The distinct evolution of d_{ac} of iPP during free stretching and die drawing at the same temperature might be caused by the calculation error and that the initial thicker lamellae without melting during die-drawing also contributed a slight larger d_{ac} at final deformation stage. Such existed difference has certain influences on the structure evolution of iPP during stretching while it did not affect the main discussion and conclusion in the current work. Although the α-nucleated iPP samples had distinct fractions of oriented parent lamellae at different temperatures during die-drawing, the orientation degrees of molecular chains of these samples registered in Fig. 4 were nearly constant. Such performances might be a result of the whole molecular chains of iPP deformed at different temperatures with a lower orientation degree. The slight increase of parent lamellae with normal parallel to the deformation direction could not lead to a significant change in the orientation degree of molecular chains.

CONCLUSIONS

The oriented cross-hatched structure evolution of die-drawn samples was revealed by employing the wide-angle X-ray technique and the tensile-stretched samples deformed at the same conditions were chosen as a reference. It turned out that not only the deformation mode, the existence of α-nucleating agents, and the deformation temperature could also affect the final parent lamellae fractions of iPP after die drawing. The die-drawing process apparently had an advantage over the tensile stretching in preserving more oriented parent-daughter of iPP. The die-induced force $F_{\perp}$ which was perpendicular to the elongation direction was the main reason for causing the lower fractions of oriented parent lamellae with normal along the deformation direction in the die-drawn samples. This effect could be enlarged when the sample was with thicker initial lamellae. So that the final oriented parent lamellae of iPP during die-drawing was influenced by the addition of α-nucleating agents and the deformation temperature. Without $F_{\perp}$, the original lamellae could be mechanically melted and the molecular chains would realign along the elongation direction for forming the new lamellae due to the sufficient stress. Hence, the influence of α-nucleating agents and the deformation temperature on the development of oriented parent lamellae disappeared in the free stretched iPP samples. This work revealed the essence of the oriented parent-daughter lamellae evolution during the die-drawing process and provided a novel entrance for regulating the oriented cross-hatched structure at solid state iPP.

ACKNOWLEDGMENTS

This work is supported by the National Natural Science Foundation of China (NO21704102, U1832186, and 51525305), Newton Advanced Fellowship of the Royal Society, United Kingdom (NA 150222) and ExxonMobil Asia Pacific Research & Development Co., Ltd. The authors acknowledge Dr. Ran Chen at Changchun Institute of Applied Chemistry who developed the MATLAB™ codes for data processing.

REFERENCES

1 Colombe, G.; Gree, S.; Lhost, O.; Dupire, M.; Rosenthal, M.; Ivanov, D. A. Correlation between mechanical properties and orientation of the crystalline and mesomorphic phases in isotactic polypropylene fibers. *Polymer* **2011**, *52*, 5630-5643.

2 Hine, P. J.; Ward, I. M.; Jordan, N. D.; Olley, R.; Bassett, D. C. The hot compaction behaviour of woven oriented polypropylene fibres and tapes. I. Mechanical properties. *Polymer* **2003**, *44*, 1117-1131.

3 Chen, X. D.; Xu, R. J.; Xie, J. Y.; Lin, Y. F.; Lei, C. H.; Li, L. B. The study of room-temperature stretching of annealed polypropylene cast film with row-nucleated crystalline structure. *Polymer* **2016**, *94*, 31-42.

4 Gohil, R. M. Morphology shrinkage relationships in semicrystalline polymers - epitaxy, a way of eliminating amorphous contribution. *Colloid Polym. Sci.* **1992**, *270*, 128-133.

5 Lu, Y.; Thompson, G.; Lyu, D.; Caton-Rose, P.; Coates, P.; Men, Y. F. Orientation direction dependency of cavitation in pre-oriented isotactic polypropylene at large strains. *Soft Matter* **2018**, *14*, 4432-4444.

6 Khoury, F. Spherulitic crystallization of isotactic polypropylene from solution - on evolution of monoclinic spherulites from dendritic chain-folded crystal precursors. *J. Res. Natl. Bur. Stand.* **1966**, *70A*, 29.

7 Padden, F. J.; Keith, H. D. Crystallization in thin films of isotactic polypropylene. *J. Appl. Phys.* **1966**, *37*, 4013-4020.

8 Binsbergen, F. L.; Delange, B. G. M. Morphology of polypropylene crystallized from melt. *Polymer* **1968**, *9*, 23-40.

9 Lotz, B.; Wittmann, J. C. The molecular-origin of lamellar branching in the alpha-(monoclinic) form of isotactic polypropylene. *J. Polym. Sci. Polym. Phys.* **1986**, *24*, 1541-1558.

10 Lotz, B.; Wittmann, J. C.; Lovinger, A. J. Structure and morphology of poly(propylenes): A molecular analysis. *Polymer* **1996**, *37*, 4979-4992.

11 Alamo, R. G.; Brown, G. M.; Mandelkern, L.; Lehtinen, A.; Paukkeri, R. A morphological study of a highly structurally regular isotactic poly(propylene) fraction. *Polymer* **1999**, *40*, 3933-3944.

12 Castelein, G.; Coulon, G.; GSell, C. Polymers under mechanical stress: Deformation of the nanostructure of isotactic polypropylene revealed by scanning force microscopy. *Polym. Eng. Sci.* **1997**, *37*, 1694-1701.

13 Dias, P.; Kazmierczak, T.; Chang, A.; Ansems, P.; Van Dun, J.; Hiltner, A.; Baer, E. Relationship of polymorphic crystalline phase texture to strain recovery and stiffness of a propylene-based elastomer. *J. Appl. Polym. Sci.* **2009**, *112*, 3736-3747.

14 Raidt, T.; Hoeher, R.; Katzenberg, F.; Tiller, J. C. Multiaxial reinforcement of cross-linked isotactic poly(propylene) upon uniaxial stretching. *Macromol. Mater. Eng.* **2017**, *302*, 1600308.

15 Meng, L. P.; Lin, Y. F.; Xu, J. L.; Chen, X. W.; Li, X. Y.; Zhang, Q. L.; Zhang, R.; Tian, N.; Li, L. B. A universal equipment for biaxial stretching of polymer films. *Chinese J. Polym. Sci.* **2015**, *33*, 754-762.

16 Nogales, A.; Mitchell, G. R. R.; Vaughan, A. S. Anisotropic crystallization in polypropylene induced by deformation of a nucleating agent network. *Macromolecules* **2003**, *36*, 4898-4906.

17 Nogales, A.; Mitchell, G. R. Development of highly oriented polymer crystals from row assemblies. *Polymer* **2005**, *46*, 5615-5620.

18 Nogales, A.; Olley, R. H.; Mitchell, G. R. Directed crystallisation of synthetic polymers by low-molar-mass self-assembled templates. *Macromol. Rapid Comm.* **2003**, *24*, 496-502.

19 Lipp, J.; Shuster, M.; Feldman, G.; Cohen, Y. Oriented crystallization in polypropylene fibers induced by a sorbitol-based nucleator. *Macromolecules* **2008**, *41*, 136-140.

20 Zhang, S.; Minus, M. L.; Zhu, L. B.; Wong, C. P.; Kumar, S. Polymer transcrystallinity induced by carbon nanotubes. *Polymer* **2008**, *49*, 1356-1364.

21 Chang, B. B.; Schneider, K.; Patil, N.; Roth, S.; Heinrich, G. Microstructure characterization in a single isotactic polypropylene spherulite by synchrotron microfocus wide angle x-ray scattering. *Polymer* **2018**, *142*, 387-393.

22 Troisi, E. M.; Caelers, H. J. M.; Peters, G. W. M. Full characterization of multiphase, multimorphological kinetics in flow-induced crystallization of ipp at elevated pressure. *Macromolecules* **2017**, *50*, 3869-3883.

23 Nozue, Y.; Shinohara, Y.; Ogawa, Y.; Sakurai, T.; Hori, H.; Kasahara, T.; Yamaguchi, N.; Yagi, N.; Amemiya, Y. Deformation behavior of isotactic polypropylene spherulite during hot drawing investigated by simultaneous microbeam saxs-waxs and pom measurement. *Macromolecules* **2007**, *40*, 2036-2045.

24 Liu, Y. P.; Hong, Z. H.; Bai, L. G.; Tian, N.; Ma, Z.; Li, X. Y.; Chen, L.; Hsiao, B. S.; Li, L. B. A novel way to monitor the sequential destruction of parent-daughter crystals in isotactic polypropylene under uniaxial tension. *J. Mater. Sci.* **2014**, *49*, 3016-3024.

25 Coates, P. D.; Ward, I. M. Drawing of polymers through a conical die. *Polymer* **1979**, *20*, 1553-1560.

26 Coates, P. D.; Caton-Rose, P.; Ward, I. M.; Thompson, G. Process structuring of polymers by solid phase orientation processing. *Sci. China Chem.* **2013**, *56*, 1017-1028.

27 Lyu, D.; Sun, Y.; Thompson, G.; Lu, Y.; Caton-Rose, P.; Lai, Y.; Coates, P.; Men, Y. Die geometry induced heterogeneous morphology of polypropylene inside the die during die-drawing process. *Polym. Test.* **2019**, *74*, 104-112.

28 Cheng, S. Z. D.; Janimak, J. J.; Zhang, A.; Hsieh, E. T. Isotacticity effect on crystallization and melting in polypropylene fractions: 1. Crystalline structures and thermodynamic property changes. *Polymer* **1991**, *32*, 648-655.

29 Kristiansen, M.; Werner, M.; Tervoort, T.; Smith, P.; Blomenhofer, M.; Schmidt, H. W. The binary system isotactic polypropylene/bis(3,4-dimethylbenzylidene)sorbitol: Phase behavior, nucleation, and optical properties. *Macromolecules* **2003**, *36*, 5150-5156.

30 Yang, X.; Tuinea-Bobe, C.; Whiteside, B.; Coates, P.; Lu, Y.; Men, Y. Molecular weight dependency of β phase formation in injection-molded isotactic polypropylene. *J. Appl. Polym. Sci.* **2019**, *136*, 48555.

31 P. Hermans; P. Platzek. Beiträge zur kenntnis des deformationsmechanismus und der feinstruktur der hydratzellulose,. *Kolloid Z.* **1939**, *88*, 68-72.

32 Polanyi, M. The x-ray fiber diagram. *Z. Phys.* **1921**, *7*, 149-180.

33 Tortorella, N.; Beatty, C. L. Morphology and crystalline properties of impact-modified polypropylene blends. *Polym. Eng. Sci.* **2008**, *48*, 1476-1486.

34 Zhu, P. W.; Edward, G. Orientational distribution of parent-daughter structure of isotactic polypropylene: A study using simultaneous synchrotron waxs and saxs. *J. Mater. Sci.* **2008**, *43*, 6459-6467.

35 Lu, Y.; Lyu, D.; Cavallo, D.; Men, Y. Enhanced beta to alpha recrystallization in beta isotactic polypropylene with different thermal histories. *Polym. Crystal.* **2019**, *2*, e10040.

36 Fujiyama, M.; Wakino, T.; Kawasaki, Y. Structure of skin layer in injection-molded polypropylene. *J. Appl. Polym. Sci.* **1988**, *35*, 29-49.

37 Kantz, M. R.; Newman, H. D.; Stigale, F. H. The skin - core morphology and structure–property relationships in injection - molded polypropylene. *J. Appl. Polym. Sci.* **1972**, *16*, 1249-1260.

38 Lu, Y.; Chen, R.; Zhao, J.; Jiang, Z. Y.; Men, Y. F. Stretching temperature dependency of fibrillation

process in isotactic polypropylene. *J. Phys. Chem. B* **2017**, *121*, 6969-6978.

39 Sadler, D. M.; Barham, P. J. Structure of drawn fibers .1. Neutron-scattering studies of necking in melt-crystallized polyethylene. *Polymer* **1990**, *31*, 36-42.

40 Men, Y. F.; Rieger, J.; Strobl, G. Role of the entangled amorphous network in tensile deformation of semicrystalline polymers. *Phys. Revi. Lett.* **2003**, *91*, 095502.

41 Aboulfaraj, M.; Gsell, C.; Ulrich, B.; Dahoun, A. In-situ observation of the plastic-deformation of polypropylene spherulites under uniaxial tension and simple shear in the scanning electron-microscope. *Polymer* **1995**, *36*, 731-742.

for Graphical Abstract use only

Advantage of preserving bi-orientation structure of isotactic polypropylene through die drawing

Dong Lyu, Ying-Ying Sun, Yu-Qing Lai, Glen Thompson, Philip Caton-Rose, Phil Coates, Ying Lu, and Yong-Feng Men

The die-drawing process preferred to preserve bi-oriented lamellae of iPP comparing to free tensile stretching. The α-nucleating agents promoted the growth of initial oriented parent-daughter lamellae of iPP, resulting in the abundant oriented cross-hatch structure after die-drawing. The force induced by the die should be responsible for the performance mentioned-above.